Supplementary Data

Table S1: Primers used for real time RT-PCR analysis. All primers written from 5' to 3' (left to right).

Gene	Forward Primer	Reverse Primer
Alpl	CAT GTA CCC GAA CAG AAC	GGG CTC AAA GAG ACC TAA GA
B2m	AAT GGG AAG CCG AAC ATA C	CCA TAC TGG CAT GCT TAA CT
Bglap	GAC CTC ACA GAT GCC AAG	CAA GCC ATA CTG GTC TGA TAG
Ppif	CCC GCT CGT GTA CTT GGA CG	CTC GTC AGG AAA GCG GCT TC

Table S2: Example of power calculation used to determine the n for biomechanical testing.

Sample Size (n)	σ (Std Dev)	Δ (effect size)	α (1-p, 5%)	β (power, 80%)
6	0.357	0.566	1.96	0.8416

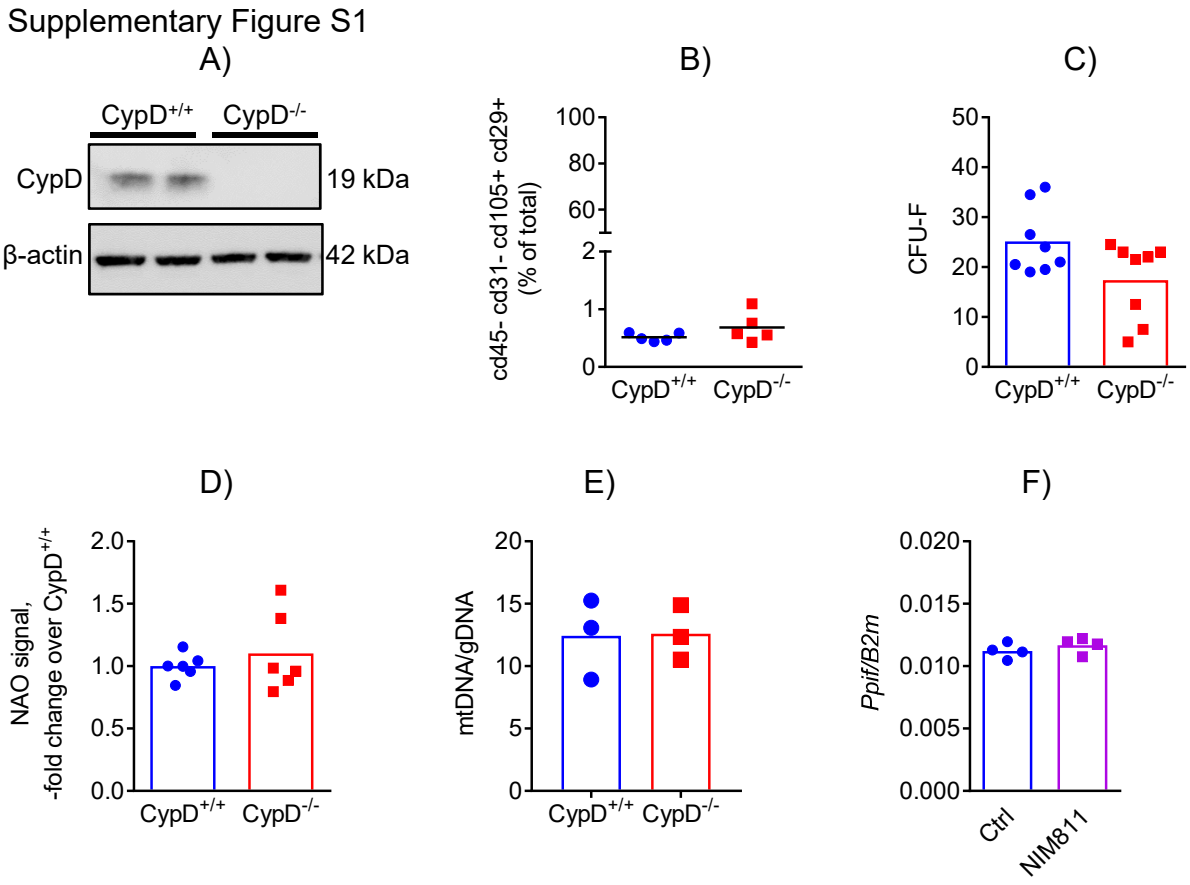

Supplementary Figure S1 (Related to Figure 1). Genetic deletion of CypD does not affect BMSC numbers or the number of mitochondria per cell. BMSCs from CypD$^{+/+}$ and CypD$^{-/-}$ littermates were analyzed by western blotting for CypD expression (A, blot is a representative of 6), by flow cytometry (B) for BMSC markers (cd45- cd31- cd105+ cd29+), or via CFU assay (C). CypD$^{-/-}$ BMSCS showed complete deletion of CypD and no difference in surface markers or CFU-F count when compared to control CypD$^{+/+}$ BMSCs. Mitochondrial mass and mtDNA copy number determined with NAO staining (D) and qPCR (E), respectively, were similar in CypD$^{+/+}$ and CypD$^{-/-}$ BMSCs. BMSCs isolated from C57BL/6J mice and treated with NIM811 (F) have similar expression of CypD gene (*Ppif*) as controls. *Ppif* expression was measured with real-time RT-PCR and normalized to *B2m* expression. Plots show actual data points and calculated means. Statistical analysis was done with unpaired *t*-test.

Supplementary Figure S2 A)

Symbol	Entrez Gene Name	Fold Change	*p*-value
Ncf4	neutrophil cytosolic factor 4	-2.18	0.007
Apoe	apolipoprotein E	-1.57	0.043
Nfkbie	NFKB inhibitor epsilon	-1.51	0.030
Nfkbia	NFKB inhibitor alpha	-1.42	0.003
Ifngr1	interferon gamma receptor 1	-1.31	0.018
Irf1	interferon regulatory factor 1	-1.27	0.031
Rhoh	ras homolog family member H	-1.26	0.026
Rhobtb1	Rho related BTB domain containing 1	-1.23	0.003
Tlr4	toll like receptor 4	-1.21	0.039
Pik3r1	phosphoinositide-3-kinase regulatory subunit 1	-1.20	0.029
Map3k14	mitogen-activated protein kinase kinase kinase 14	-1.19	0.001
Nfkb1	nuclear factor kappa B subunit 1	-1.16	0.030
Nfkb2	nuclear factor kappa B subunit 2	-1.16	0.048
Nfkbib	NFKB inhibitor beta	-1.16	0.036
Rhoj	ras homolog family member J	-1.13	0.038
Rela	RELA proto-oncogene, NF-kB subunit	-1.12	0.018
Ppp2r1a	protein phosphatase 2 scaffold subunit Aalpha	-1.09	0.001
Map3k3	mitogen-activated protein kinase kinase kinase 3	-1.08	0.046
Map2k4	mitogen-activated protein kinase kinase 4	-1.08	0.035
Ppp1r12a	protein phosphatase 1 regulatory subunit 12A	-1.06	0.029
Akt2	AKT serinethreonine kinase 2	-1.05	0.023
Jak1	Janus kinase 1	-1.04	0.009

B)

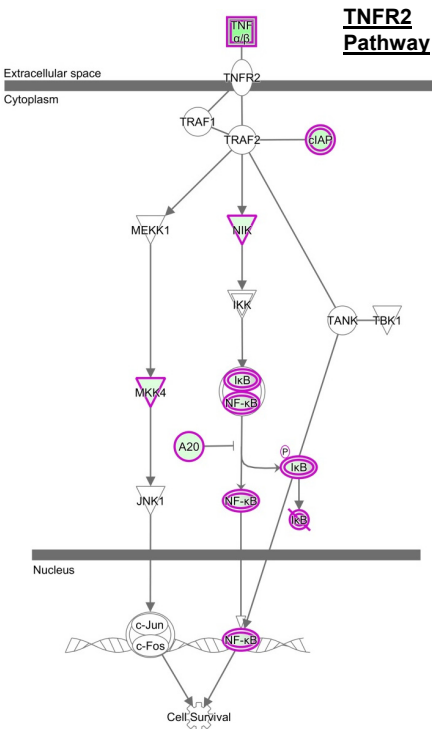

C)

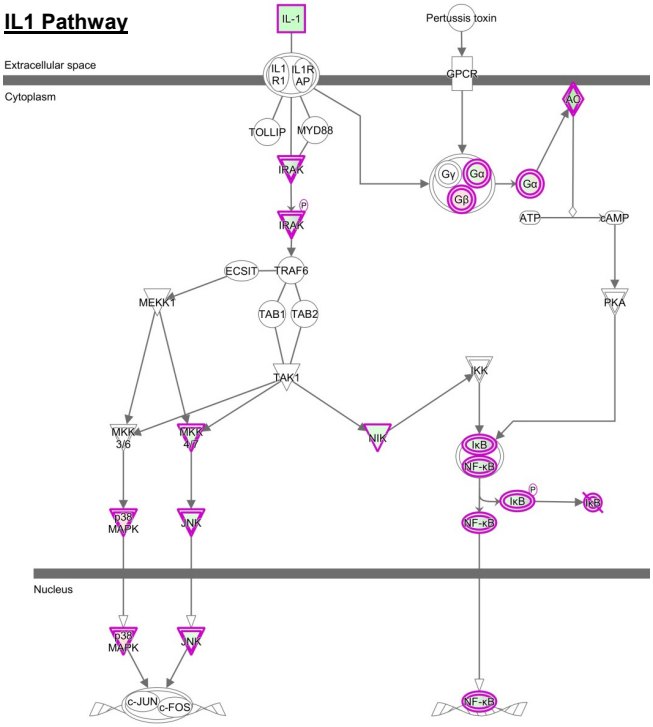

Supplementary Figure S2 (Related to Figure 2). CypD KO BMSCs show anti-inflammatory phenotype. BMSCs from CypD$^{-/-}$ and control CypD$^{+/+}$ littermates (n=3) were cultured in growth media and analyzed by RNAseq followed by Ingenuity Pathway Analysis. The analysis indicated an anti-inflammatory phenotype in CypD$^{-/-}$ BMSCs as evident from significant downregulation of many inflammatory genes (A) and of major inflammatory pathways, TNFR2 (B) and IL1 (C). Statistical analysis was done with unpaired *t*-test.

Supplementary Fig. S3

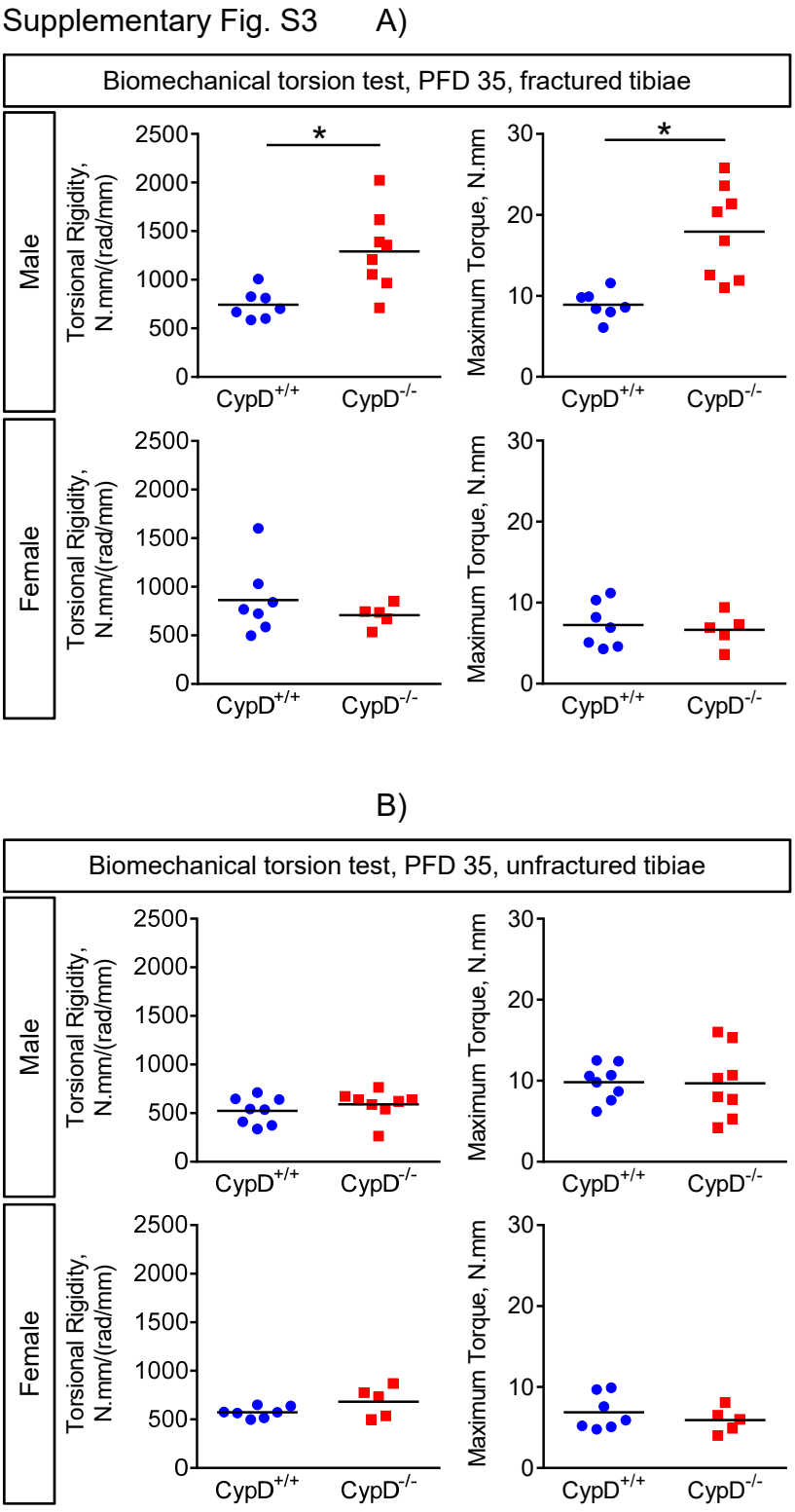

Supplementary Figure S3 (related to Figure 4). Genetic deletion of CypD results in stronger repaired bone in male mice at post fracture day 35 and no difference in unfractured bone. Tibial fractures were performed on 3-month-old male and female mice; and contralateral unfractured bones were collected for torsion testing at PFD 35. Biomechanical properties were reported as torsional rigidity and maximum torque. $CypD^{-/-}$ male but not female mice show tougher and stronger bone repair at PFD 35. No difference in torsional properties of contralateral unfractured bone when compared to control $CypD^{+/+}$ littermates is observed in both males and females. Plots show actual data points and calculated means. *, $p < 0.05$ vs $CypD^{+/+}$ controls as determined by an unpaired *t*-test.

Supplementary Fig. S4

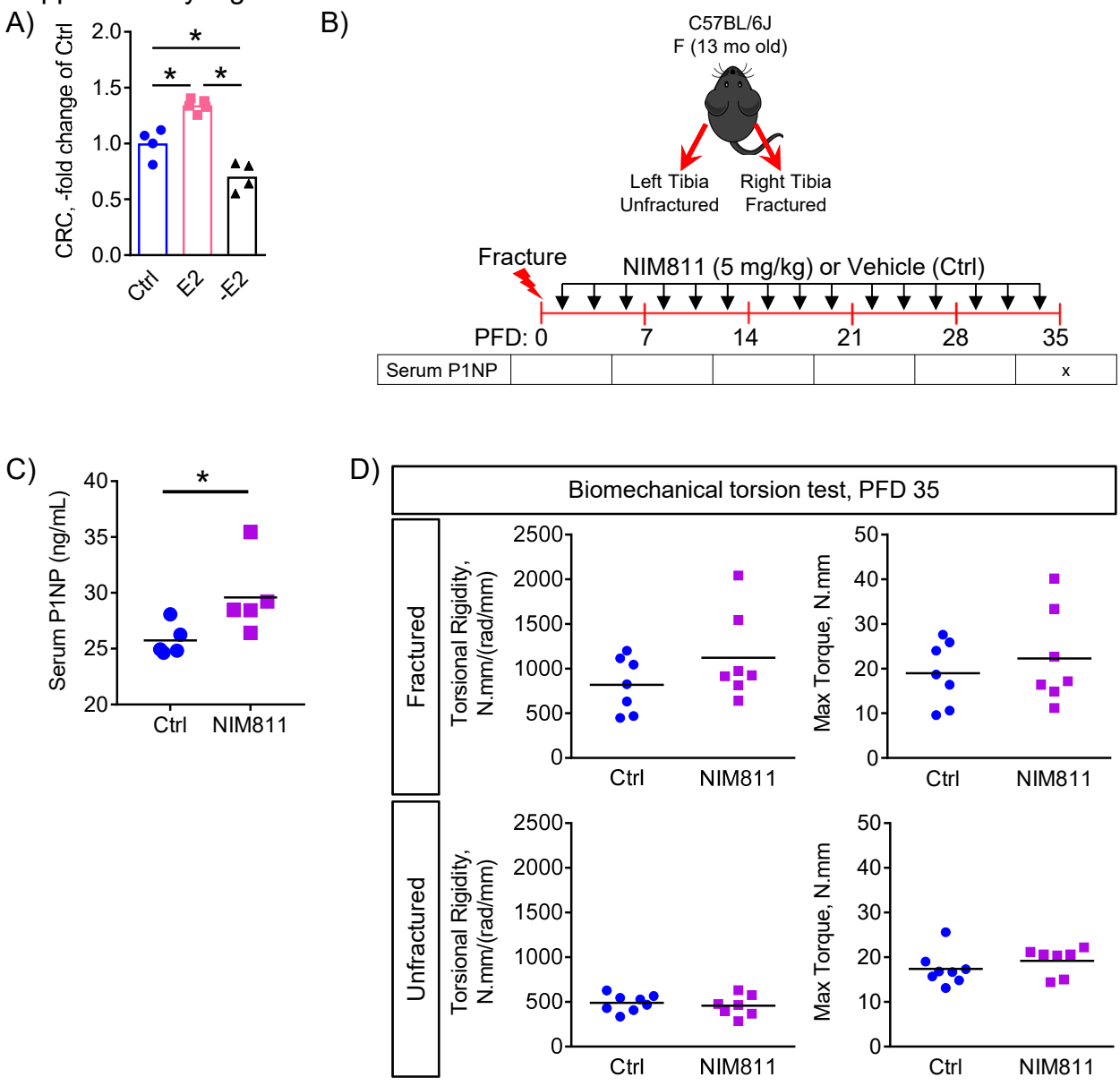

Supplementary Figure S4 (Related to Figure 4). Effect of estrogen on mitochondria in BMSCs and of NIM811 on bone repair in mice. A) BMSCs, either pre-treated with estradiol (E2) at 10 nM or incubated in estrogen-depleted media (-E2), were subjected to calcium retention capacity (CRC) assay. E2 increases CRC and, thus inhibits MPTP opening; B) Tibial fractures were performed on 13-month-old C57BL/6J female mice which were then treated with NIM811 or vehicle. Serum collected at PFD 35 for P1NP bone formation marker assay which shows an increase in NIM811 group indicating increased bone formation (C); D) Tibial fractures were performed on 3-month-old C57BL/6J male mice which were then treated with NIM811 or vehicle. Plots show actual data points and calculated means. *, $p < 0.05$ as determined by ANOVA followed by post-hoc analysis (A) or unpaired *t*-test (C & D).

Supplementary Fig. S5

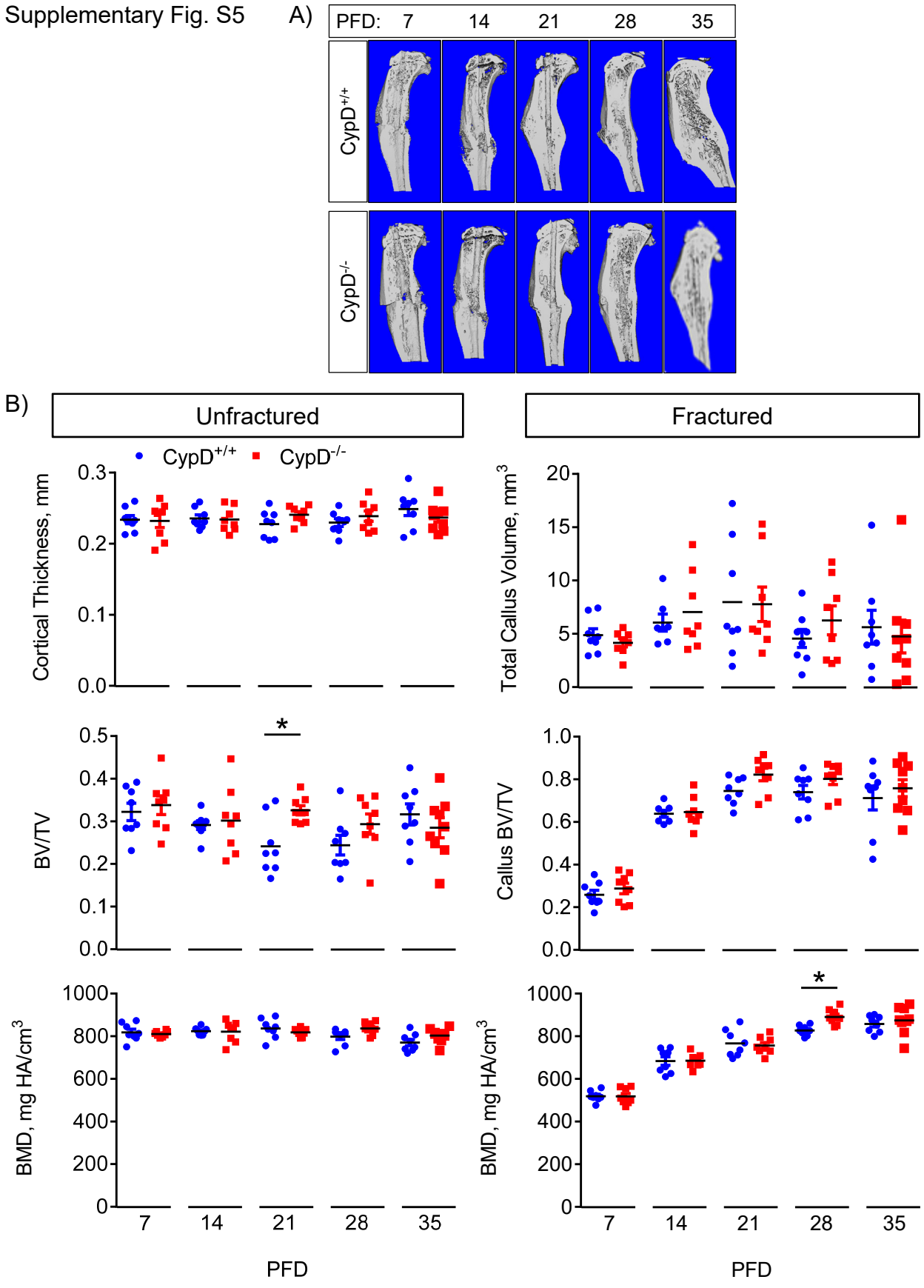

Supplementary Figure S5 (related to Figure 5). Micro-CT analysis of calluses during fracture healing. Fractured tibiae were collected at various time points and analyzed with micro-CT. Sagittal sections of the fractured tibiae are shown in A. In contralateral unfractured tibia, most of the parameters were similar in $CypD^{+/+}$ and $CypD^{-/-}$ mice except for trabecular BV/TV at PFD 21 (B, middle left panel). In the fractured tibiae, most of the parameters were similar in $CypD^{+/+}$ and $CypD^{-/-}$ mice apart from BMD at PFD 28 (B, bottom right panel). Plots show actual data points and calculated means. *, $p < 0.05$, determined by unpaired *t*-test of each time point. *t*-test was used because samples at each time point were collected and analyzed independently of other time points.

Supplementary Fig. S6

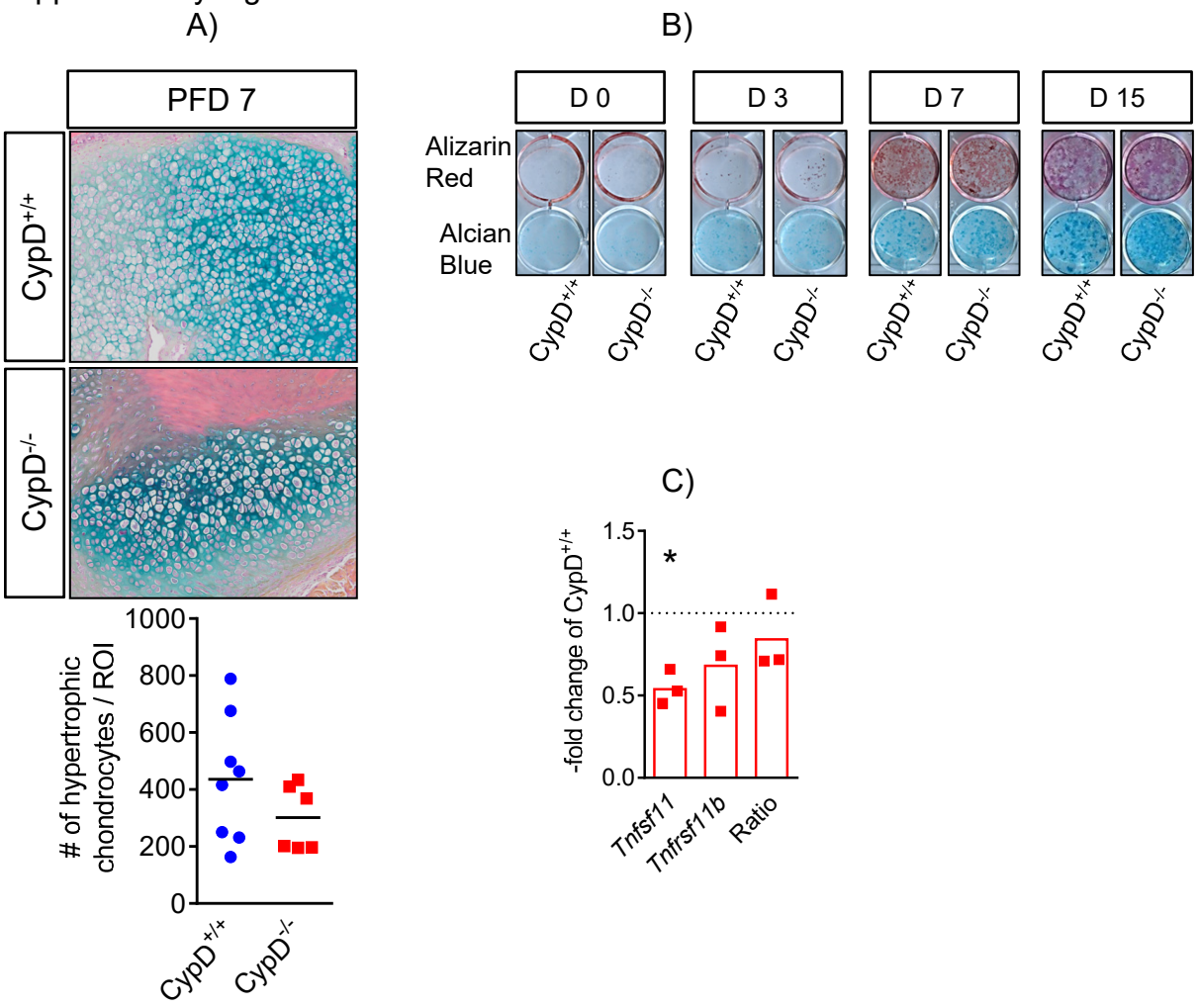

Supplementary Figure S6 (Related to Figures 6 & 7). Effect of CypD deletion on cartilage and remodeling factors. A) CypD$^{+/+}$ and CypD$^{-/-}$ fracture callus cartilage was examined for chondrocyte hypertrophy. No significant differences in the number of hypertrophic chondrocytes between CypD$^{+/+}$ and CypD$^{-/-}$ mice were observed; B) BMSCs were incubated in chondrocyte maturation/hypertrophy media and specific staining for maturation (Alcian Blue) and hypertrophy-associated mineralization (Alizarin Red) was performed. No differences were observed between CypD$^{+/+}$ and CypD$^{-/-}$ BMSCs. Images are representatives of 4; C) CypD$^{-/-}$ BMSCS showed no difference in the ratio of RANKL gene (*Tnfsf11*) to Opg gene (*Tnfrsf11b*) expression when compared to control CypD$^{+/+}$ BMSCs. Plots show actual data points and calculated means. *, $p < 0.05$ as determined by unpaired *t*-test.

Supplementary Fig. S7

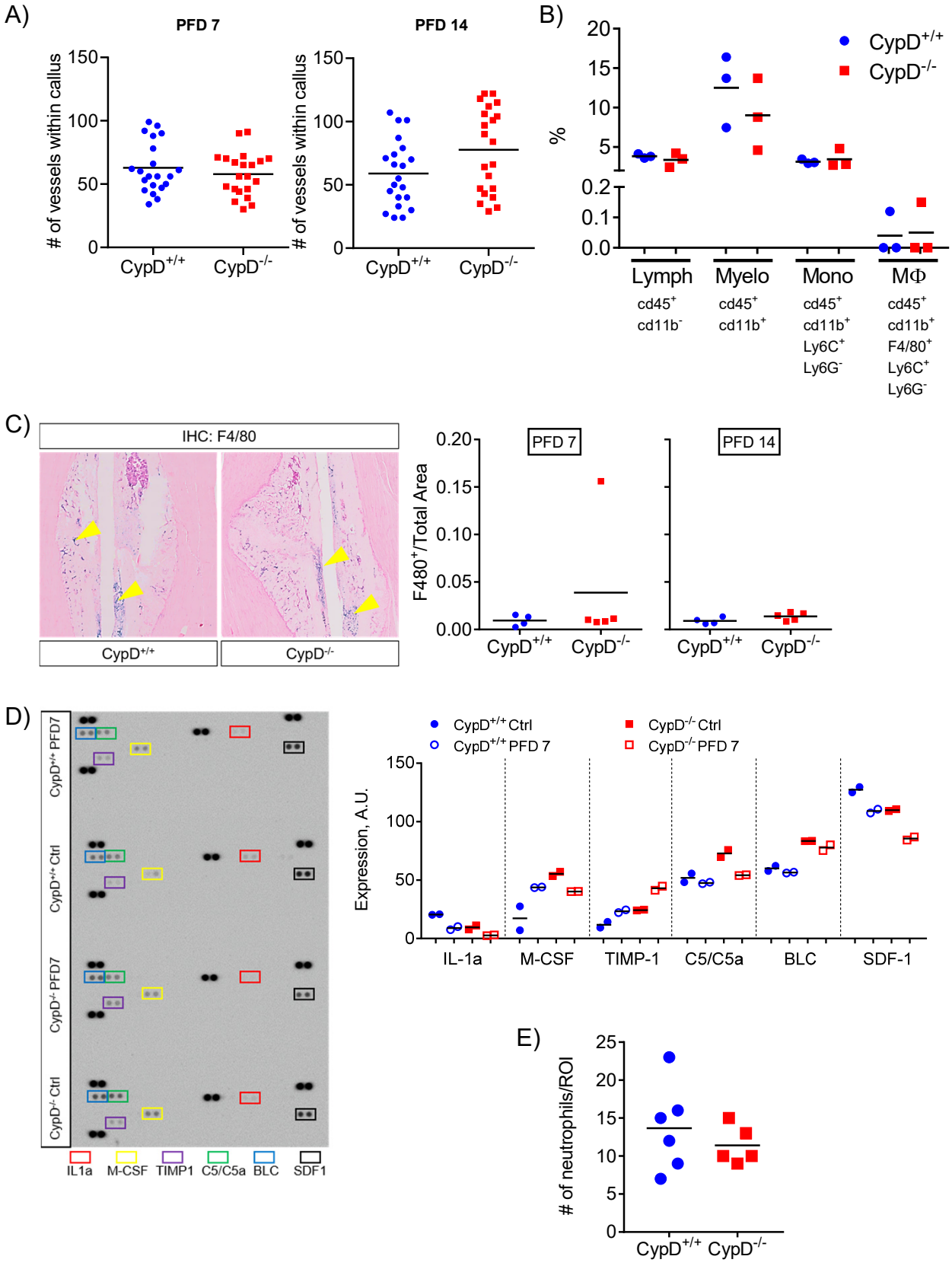

Supplementary Figure S7 (related to Figure 7). Genetic deletion of CypD does not affect fracture callus vascularization or immune cells. A) Fractured tibiae were collected at PFD7 and 14 and then analyzed via ABH/OG histology followed by histomorphometry analysis for vessels. $CypD^{-/-}$ mice show no difference in vessel number at PFD7 (A) or PFD14 (B) when compared to $CypD^{+/+}$ control littermates; B) Bone marrow was analyzed for immune cell phenotype using flow cytometry; C) Macrophages in fracture calluses were identified using F4/80 immunostaining; D) Serum cytokines at PFD 0 and 7 were detected using ELISA;E) Neutrophils infiltrating fracture calluses were identified by specific morphology and counted. In (B) – (E) no significant differences between $CypD^{+/+}$ and $CypD^{-/-}$ mice were observed. Plots show actual data points and calculated means.

Supplementary Figure S8

A)

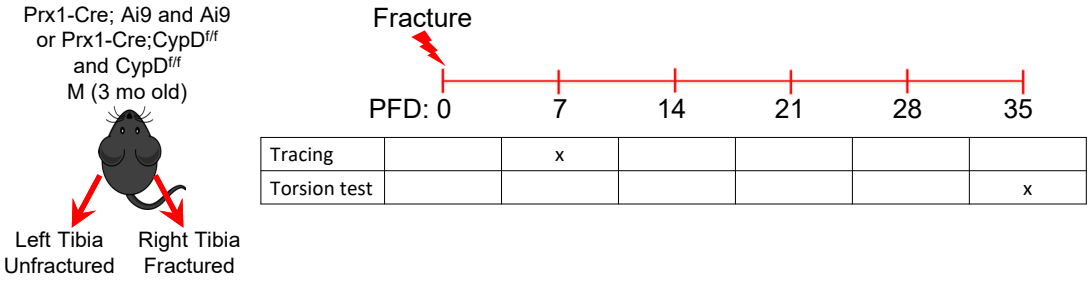

Tracing		x				
Torsion test						x

B)

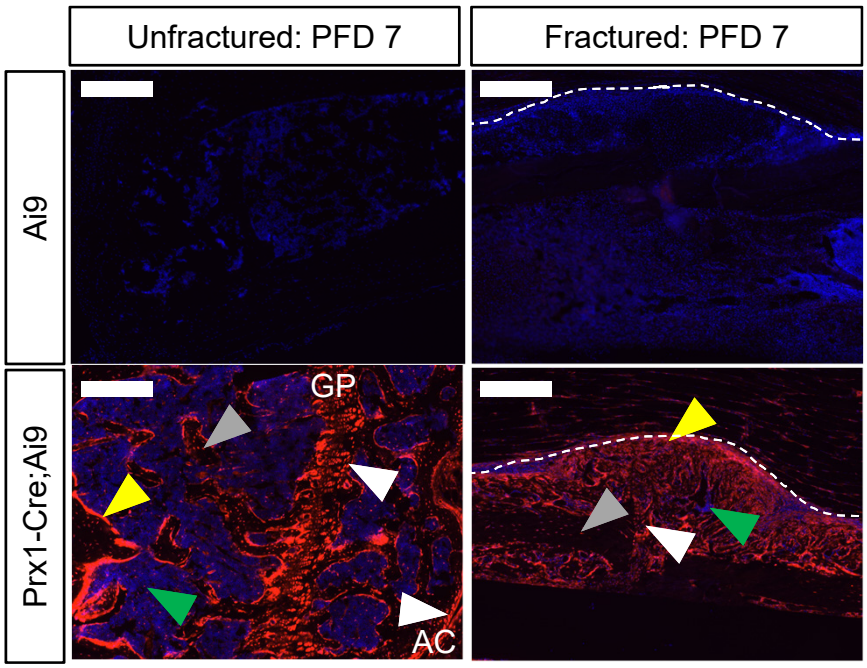

C)

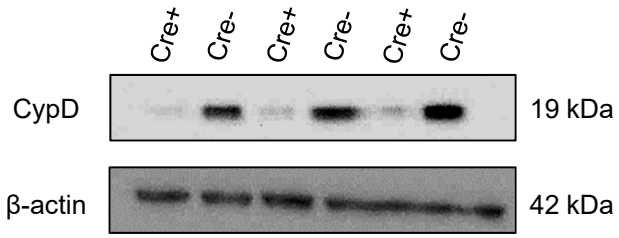

D)

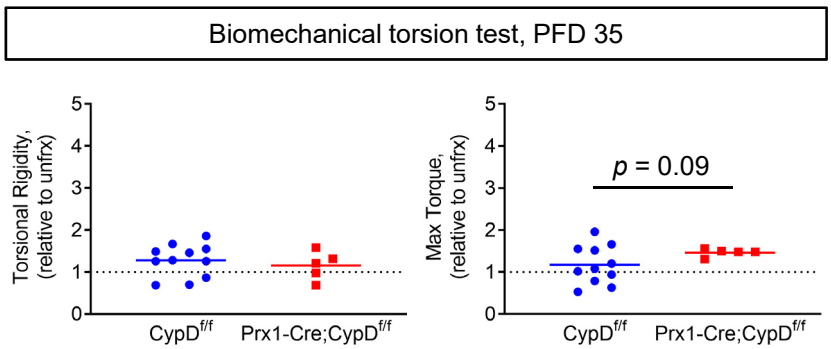

Supplementary Figure S8. BMSC-specific deletion of CypD is not sufficient to promote bone fracture repair. BMSC and BMSC-progeny specific Prx1-Cre driver was used to perform lineage tracing with Ai9 (tdTomato) reporter and tissue-specific CypD deletion in $CypD^{f/f}$ mice. A) Tibial fracture was induced; and calluses were analyzed for Prx1-Cre specificity at PFD 7 and with biomechanical torsion test at PFD 35; B) Ai9 positivity in Cre^{+} (bottom panels) but not Cre^{-} (top panels) mice confirms Prx1 specificity in BMSC lineage. In the unfractured tibia (bottom left panel), Prx1-Cre-driven Ai9 labels BMSCs in the bone marrow (green arrowhead), osteoblasts (yellow arrowhead), osteocytes (gray arrowhead), as well as chondrocytes (white arrowhead) in the articular cartilage (AC) and growth plate (GP). The same labeling is seen in fracture callus (bottom right panel); C) CypD knock-down in Cre^{+} but not Cre^{-} $CypD^{f/f}$ BMSCs was confirmed with western blotting; D) Biomechanical properties of repaired tibiae were measured at PFD 35. Data are expressed as relative to the contralateral unfractured limb to account for potential differences in bone phenotype between animals. No significant differences between Cre^{+} and Cre^{-} mice were observed as determined by an unpaired *t*-test. Plots show actual data points and calculated means.